



Atmospheric stability and complex terrain: comparing measurements and CFD

Koblitz, Tilman; Bechmann, Andreas; Berg, Jacob; Sogachev, Andrey; Sørensen, Niels N.; Réthoré, Pierre-Elouan

Published in:
Journal of Physics: Conference Series (Online)

Link to article, DOI:
[10.1088/1742-6596/555/1/012060](https://doi.org/10.1088/1742-6596/555/1/012060)

Publication date:
2014

Document Version
Publisher's PDF, also known as Version of record

[Link back to DTU Orbit](#)

Citation (APA):
Koblitz, T., Bechmann, A., Berg, J., Sogachev, A., Sørensen, N. N., & Réthoré, P-E. (2014). Atmospheric stability and complex terrain: comparing measurements and CFD. *Journal of Physics: Conference Series (Online)*, 555, [012060]. <https://doi.org/10.1088/1742-6596/555/1/012060>

General rights

Copyright and moral rights for the publications made accessible in the public portal are retained by the authors and/or other copyright owners and it is a condition of accessing publications that users recognise and abide by the legal requirements associated with these rights.

- Users may download and print one copy of any publication from the public portal for the purpose of private study or research.
- You may not further distribute the material or use it for any profit-making activity or commercial gain
- You may freely distribute the URL identifying the publication in the public portal

If you believe that this document breaches copyright please contact us providing details, and we will remove access to the work immediately and investigate your claim.

Atmospheric stability and complex terrain: comparing measurements and CFD

This content has been downloaded from IOPscience. Please scroll down to see the full text.

2014 J. Phys.: Conf. Ser. 555 012060

(<http://iopscience.iop.org/1742-6596/555/1/012060>)

View [the table of contents for this issue](#), or go to the [journal homepage](#) for more

Download details:

IP Address: 192.38.90.17

This content was downloaded on 19/12/2014 at 11:18

Please note that [terms and conditions apply](#).

Atmospheric stability and complex terrain: comparing measurements and CFD

T Koblitz, A Bechmann, J Berg, A Sogachev, N Sørensen and P-E Réthoré

DTU Wind Energy, DK-4000 Roskilde, Denmark

E-mail: tiko@dtu.dk

Abstract. For wind resource assessment, the wind industry is increasingly relying on Computational Fluid Dynamics models that focus on modeling the airflow in a neutrally stratified surface layer. So far, physical processes that are specific to the atmospheric boundary layer, for example the Coriolis force, buoyancy forces and heat transport, are mostly ignored in state-of-the-art flow solvers. In order to decrease the uncertainty of wind resource assessment, the effect of thermal stratification on the atmospheric boundary layer should be included in such models. The present work focuses on non-neutral atmospheric flow over complex terrain including physical processes like stability and Coriolis force. We examine the influence of these effects on the whole atmospheric boundary layer using the DTU Wind Energy flow solver EllipSys3D. To validate the flow solver, measurements from Benakanahalli hill, a field experiment that took place in India in early 2010, are used. The experiment was specifically designed to address the combined effects of stability and Coriolis force over complex terrain, and provides a dataset to validate flow solvers. Including those effects into EllipSys3D significantly improves the predicted flow field when compared against the measurements.

1. Introduction

Most Computational Fluid Dynamics (CFD) solvers applied for atmospheric flows focus primarily on modeling the airflow in a neutrally stratified surface layer. In order to decrease the uncertainty, especially in complex terrain, the effect of stability and Coriolis force on the atmospheric boundary layer (ABL) should be included in such models. To get an appropriate description of the whole ABL, the DTU Wind Energy CFD solver EllipSys3D [1–3] is therefore modified accordingly.

To validate the CFD solver and to get a better understanding of the influences of stability and Coriolis force on the resulting ABL flow over complex terrain, atmospheric experiments on full scale are necessary. Benchmark literature for these cases is, however, scarce. Various experiments are available that have been focusing on neutral flow over flat and complex terrain, e.g. the Askervein Hill experiment [4], or more recently the Bolund experiment [5, 6]. To validate non-neutral CFD solvers, however, large scale field experiments that capture the combined non-linear effects of stability and Coriolis force over complex terrain are needed. The Benakenahalli field experiment was specifically designed to provide such a benchmark dataset. The topography and location of the site is well suited to study the interplay of these effects. To simulate the airflow over Benakanahalli hill, the EllipSys3D solver is modified to get a more appropriate description of the whole ABL.



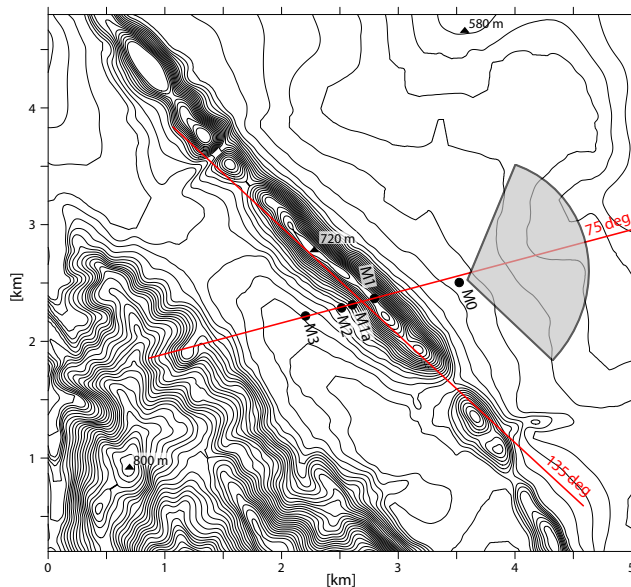


Figure 1. Contour map of surrounding terrain including mast positions. The five masts M0, M1, M1a, M2 and M3 are erected along a 75° transect. M0 is used as a reference mast for easterly winds. The considered wind direction of the present study is 135° . The shaded area indicates wind directions with near homogeneous inflow conditions.

The solver was initially developed for simulating the near-ground surface-layer flow inside a neutrally stratified domain and has under these conditions been validated against field experiments [6, 7]. In connection with a previous study the effects of stability and Coriolis force were implemented into the CFD solver [8]: the energy equation in terms of the potential temperature was solved parallel to the RANS equations, and a modified $k-\epsilon$ turbulence model was used. Computational tests validate the applicability of the modifications.

Having demonstrated the modifications necessary to model the non-neutral ABL over flat terrain, the focus of the present study is to analyze the combined effects of stability and Coriolis force over complex terrain. Simulation results over the Benakanahalli hill are presented and compared against measurements. The field experiment took place from February to April 2010. Five 80 m masts were installed along a 120 m high natural ridge equipped with sonic anemometers at five different heights and temperature sensors at the upstream mast (see Figure 1).

The first part of this paper describes the field experiment and the second part focuses on modeling the ABL flow over Benakanahalli hill. Section 2 provides a brief outline of the experiment and the resulting dataset. In Section 3 the modeling approach and the modifications implemented into EllipSys3D are briefly described. Finally section 4 presents simulation results over Benakanahalli hill for different stability classes compared against measurements. Discussion and concluding remarks are given in section 5 and 6.

2. The Benakanahalli Experiment

In early 2010 a yet unpublished field experiment took place close to the village of Benakanahalli in the region of Karnataka, India, focusing on micro meteorological properties important for wind energy. The field experiment is in many ways the natural successor to the Bolund hill experiment [6]. Bolund, a 12 m sharp edged hill, proved suitable for validation of flow models in neutral condition, while the measurements at Benakanahalli can be used to study the influence of non-neutral stratification and Coriolis force on the flow. The experiment was planned and conducted as a joint collaboration between DTU Wind Energy and Vestas Technology R&D.

2.1. Site Description

The experimental site is located 15 km southeast of the village of Benakanahalli ($14^\circ 10' 34''$ N, $75^\circ 50' 29''$ E), and the measurements were conducted from 1st of February to 6th of April 2010.

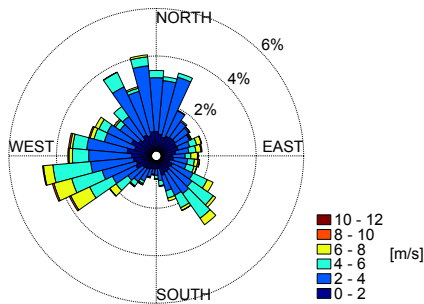


Figure 2. Distribution of wind directions at 75 m at M0. Numbers denote frequency while colors correspond to wind speeds.

Five 80 m masts were erected along a 75° transect across a long almost two-dimensional 120 m high natural ridge with slopes of around 30° , the Benakanahalli hill (see Figure 1). All five masts were equipped with sonic anemometers at five different heights. In addition temperature sensors were mounted on the upstream mast M0 and in the soil nearby. Together with measurements of heat flux from the sonic anemometers a good estimate of the thermal stratification is thus obtained. The surrounding terrain is shown in figure 1. There is a small village to the north, while the eastern and southern directions are mainly covered by farmland: rice fields, corn plants and patches of palms trees. This corresponds to a surface roughness of approximately $z_0 = 0.1$ m. Based on the inspection of the landscape the wind coming from between 35° and 135° were considered to have flat and close to homogeneous upstream conditions (indicated by shaded area in figure 1). This is ideal from a modeling perspective where simple upstream conditions are desired for validation purposes. Close to the 135° direction, however, the incoming wind shows slight perturbations from the otherwise ideal homogeneous conditions: small hills and a lake that are encountered 4-6 km upstream lead to internal boundary layers and enhanced turbulence.

2.2. General Wind Climate

In figure 2 the wind rose measured by the sonic at 75 m at mast M0 is presented. The experiment was designed for easterly winds and the transect was chosen accordingly. During the experiment, however, the wind blew predominantly from westerly and south easterly directions. With the instrumented transect located at 75° the experiment has not been ideal with only a fraction of the wind coming from this direction. The prevailing west-southwest wind direction is, from a modeling point of view, far from ideal, since the wind accelerates downhill from high elevations to the west, resulting in non-homogeneous upstream conditions. General for all wind directions is the very low wind speed (typically less than 4 m/s) and relatively high turbulence levels (larger than 20 %) due to the large surface roughness of the terrain. Having low wind speeds together with a very pronounced daily cycle of surface temperature, the wind is strongly affected by thermal stratification.

To validate the CFD solver, a dataset of three consecutive days is extracted from the measurements with winds coming from the 135° direction. The available 10 min data is averaged so that the whole period from the 5th to the 8th of February is combined in one diurnal cycle that is representative for the selected period. As mentioned above, the incoming wind for the chosen 135° direction is not perfectly horizontally homogeneous. It passes some small hills and a lake 4-6 km upstream.

Figure 3 shows the averaged daily variations of wind speed and temperature at mast M0 during the selected period. Unstable conditions occur during daytime (8:00-17:00) with a temperature maximum at around 16:00 and stable conditions are found during night (19:00-7:00) which roughly coincides with local sunrise and sunset at around 7:00 and 18:30. The observed soil temperature in figure 3 shows less amplitude than the 10 m temperature, which is caused by a higher heat capacity of the ground. The almost perfect sinusoidal shape makes

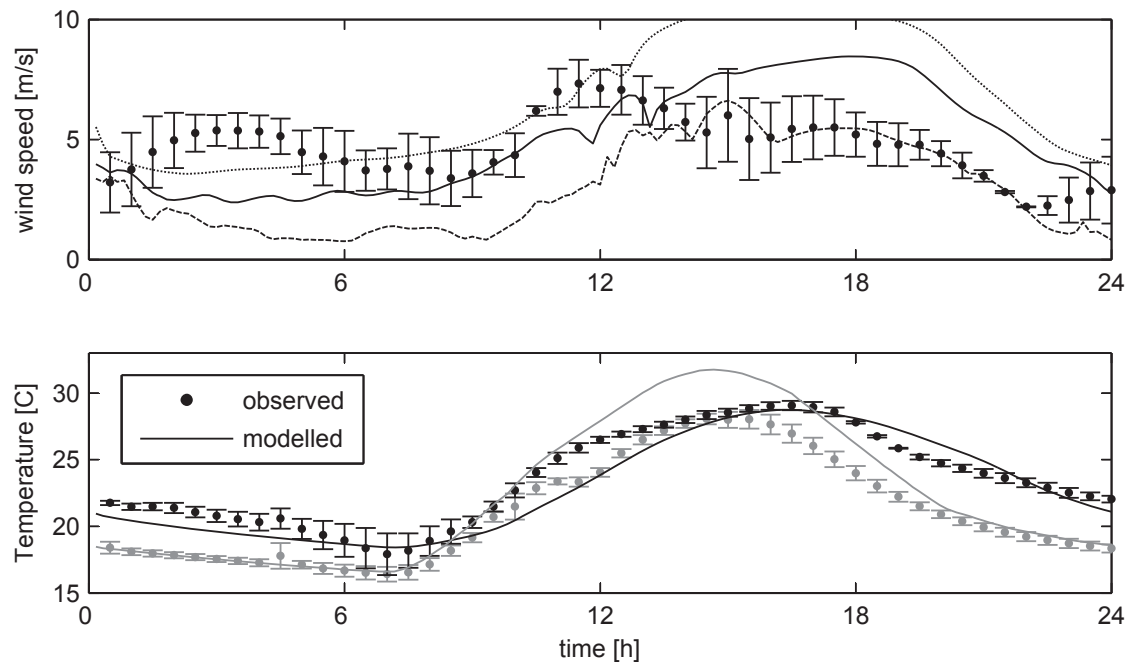


Figure 3. Time series of modeled and observed data at mast M0. The observed data represents a 3 day average shown with the corresponding error bars. Top: wind speed at 75 m height. Model results are shown for different geostrophic winds: 10 m/s (dashed line), 14 m/s (solid line) and 18 m/s (dotted line). Bottom: temperature at 10 m height (black), and surface temperature (grey). Observed soil temperature is measured 2 cm in the ground.

the temperature ideal for modeling purposes. The key dimensionless numbers of the site are the Froude number ($Fr = 0.2$) and the Rossby number ($Ro = 50/400$ day/night) with a local Coriolis parameter of $f_c = 3.57 \cdot 10^{-5}$ 1/s.

3. Modeling

The starting point for the present study is the DTU Wind Energy CFD solver EllipSys3D (from now on referred to as the neutral base solver). To model the airflow within the ABL more appropriately, the finite-volume code is modified by including the effects of the Coriolis force (induced by the rotation of the earth) and buoyancy. The CFD solver is based on the solution of the RANS equations, and the applied turbulence model is a modified version of the popular $k-\epsilon$ turbulence model [11] that was initially developed by [13], capable of representing non-neutral conditions. The modification to the CFD solver are only described in brief here. Details can be found in [8] where computational tests validate the applicability of the modifications by comparing against previous simulations [10, 14, 15] and observations [16, 17].

To include buoyancy effects, an equation for the energy in terms of the potential temperature is solved in addition to the RANS equations. The temperature equation couples with the momentum equation via vertical buoyancy forces (induced by the gravitational acceleration), and with the turbulence model via additional buoyancy terms. The buoyancy forces are added explicitly to the momentum equation as external forces. This approach can generate a numerical decoupling between the pressure and the velocities. To avoid this an algorithm for allocating discrete forces is used following [18]. The modified version of the $k-\epsilon$ turbulence model uses additional buoyancy terms [10, 19] and employs a limiter on the resulting length-scale [14]. Also ambient floor values for the turbulence variables are imposed in order to avoid numerical

issues due to turbulence values close to zero [20]. The two modified transport equations for the turbulent kinetic energy k and the dissipation ϵ read:

$$\frac{\partial k}{\partial t} + U_j \frac{\partial k}{\partial x_j} - \frac{\partial}{\partial x_i} \left(\frac{K}{\sigma_k} \frac{\partial k}{\partial x_i} \right) = P - \epsilon + B, \quad (1)$$

$$\frac{\partial \epsilon}{\partial t} + U_j \frac{\partial \epsilon}{\partial x_j} - \frac{\partial}{\partial x_i} \left(\frac{K}{\sigma_\epsilon} \frac{\partial \epsilon}{\partial x_i} \right) = \frac{\epsilon}{k} (C_{\epsilon 1} P - C_{\epsilon 2} \epsilon + C_{\epsilon 3} B), \quad (2)$$

where x_i ($x_1 = x$, $x_2 = y$, $x_3 = z$) are the longitudinal, lateral and vertical directions. U_i is the mean velocity component along x_i , K is the eddy viscosity, σ_k and σ_ϵ are the Prandtl numbers for k and ϵ respectively and P is the production of k due to shear. $C_{\epsilon 1}$, $C_{\epsilon 2}$ and $C_{\epsilon 3}$ are model coefficients. The buoyancy term B depends on the eddy viscosity and the vertical temperature gradient. In unstable conditions B is positive and appears as a source term, while B turns negative in stable conditions and acts as a sink term. The additional coefficient $C_{\epsilon 3}$ has to be quantified a priori, and an optimal value is unknown [11]. In the present case $C_{\epsilon 3} = 1$ is used. This approach is generally applicable, without trying to fit $C_{\epsilon 3}$ to single observations. The resulting eddy viscosity, K , and the mixing length, l , are expressed as

$$K = C_\mu \frac{k^2}{\epsilon}, \quad (3)$$

$$l = C_\mu^{3/4} \frac{k^{3/2}}{\epsilon}, \quad (4)$$

where C_μ is a model coefficient. All presented calculations use the set of consistent closure coefficients for ABL flows stated in table 1 below.

Table 1. k - ϵ turbulence model coefficients for standard ABL flows.

$C_{\epsilon 1}$	$C_{\epsilon 2}$	$C_{\epsilon 3}$	C_μ	σ_k	σ_ϵ
1.21	1.92	1	0.03	1.0	1.3

In the calculations the coefficient $C_{\epsilon 1}$ is replaced by a modified coefficient $C_{\epsilon 1}^*$ during the simulation following [14]:

$$C_{\epsilon 1}^* = \left[C_{\epsilon 1} + (C_{\epsilon 2} - C_{\epsilon 1}) \frac{l}{l_{max}} \right]. \quad (5)$$

This modification was initially proposed by [14] and effectively limits the maximum mixing length reached during the simulation and accounts for the weakness of the k - ϵ model to strongly overestimate the mixing length near the top of the ABL [9], while still being consistent with the standard model close to the ground. Again, no additional coefficients are introduced and the formulation only depends on the standard closure coefficients in table 1. The value of l_{max} is estimated by [21]:

$$l_{max} = 0.00027 \cdot U / f_c, \quad (6)$$

where U is the geostrophic wind and f_c is the Coriolis parameter.

In the present simulations the airflow is driven by a pressure gradient that gives the geostrophic wind velocity components $(u_g, v_g) = 1/(\rho f) (\partial p / \partial y, \partial p / \partial x)$ where ρ is the air density,

$f_c = 2\Omega \sin\lambda$ is the Coriolis parameter (with the earth's rotation rate Ω and the latitude λ) and p is the pressure.

To include Coriolis effects into the EllipSys3D solver, the Coriolis force is simply added explicitly to the momentum equations as an external force, $F_{C,i} = f_c u_j m$ where u_j denotes the velocity field and m is the mass. The Coriolis force in vertical direction is neglected. Within all subsequent simulations of the ABL, the airflow is subjected to the Coriolis force.

In order to improve convergence for small mixing lengths, ambient floor values for the turbulence variables are imposed following [20]. Especially during stable conditions at night the mixing length and the eddy viscosity approach values close to zero. To avoid numerical issues k and ϵ are not allowed to drop below a predefined limit. The set of ambient values was chosen to be $k_{amb} = 1 \cdot 10^{-4}$ and $\epsilon_{amb} = 7.2 \cdot 10^{-7}$ in all simulations, which leads to a negligible added eddy viscosity of $K = 4 \cdot 10^{-4}$ (Equation 3) on top, where the turbulence values approach their ambient levels.

4. Results

The aim of the present work is to study the combined effects of stability and Coriolis force over complex terrain, and to validate their representation in the model. The modified CFD solver presented in section 3 is used to simulate the airflow over the Benakanahalli hill and the resulting surface winds are compared against observations. The simulations are divided in two parts: first, a precursor simulation simulates a typical diurnal cycle for the ABL over flat terrain. The goal is to reconstruct the vertical structure of the flow field for different stabilities as observed at M0. In a second step, the results obtained from the precursor simulation are used to specify the initial and transient boundary conditions for the Benakanahalli hill domain. The central goal is to examine how well the modified CFD solver performs in representing non-neutral ABL flows compared to measurements and the neutral base model.

4.1. Precursor Simulation

To simulate a typical diurnal cycle at the given site a flat computational domain is used. The height of the domain is 6 km using a grid of 192 vertically stretched cells (0.08 m cell height at wall; 140 m cell height at top boundary). In horizontal directions the domain is 1 x 1 km large with a grid of 24 evenly distributed cells. A rough wall boundary condition [7] with a constant roughness of $z_0 = 0.11$ m is used, and a symmetry condition (no-gradient) on top. All vertical boundaries are cyclic. Simple forcings are applied to simulate the diurnal cycle in the ABL: a constant pressure gradient dictates a constant geostrophic wind and a prescribed cyclic variation of the surface temperature imposes different stabilities. The Coriolis parameter is $f_c = 3.57 \cdot 10^{-5}$ 1/s and the maximum length-scale is $l_{max} = 106$ m (see Equation 6) with a geostrophic wind of $u_g = 14$ m/s. The initial conditions for the simulation are computed by a steady-state simulation of a stably stratified ABL where the initial potential temperature field is described by: $\Theta = 299$ below 1 km height, and $\partial\Theta/\partial z = 3.5$ K/km above. A transient simulation is continued for five days using a 1 s numerical timestep. After simulating three consecutive days an approximately cyclic variation is obtained. The results are tested and validated by means of grid sensitivity and convergence studies.

Figure 3 shows the modeled and observed evolution of the velocity at 75 m and the temperature at 10 m at mast M0. Since the observed soil temperature has less amplitude than the 10 m temperature, the wall temperature to force our model was adjusted in order to match the observed temperature at 10 m (grey line in figure 3). The resulting modeled temperature at 10 m therefore follows the observed temperature well, having the same amplitude and a similar distribution of minima and maxima (black line in figure 3).

The observations show a decrease of wind speed around noon before the maximum temperature is reached at 16:00. This decrease of wind speed is delayed in the modeled

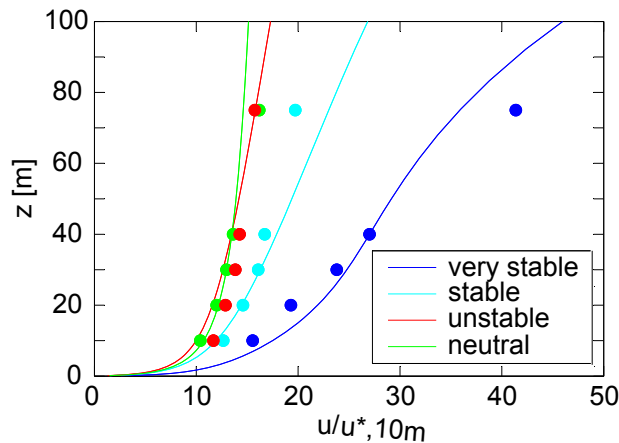


Figure 4. Averaged dimensionless velocity profiles for different stability classes. Stability conditions for both modeled and observed results are categorized based on the Monin-Obukhov length. very stable: $z/L > 0.2$; stable: $1 \cdot 10^{-3} < z/L < 0.2$; neutral: $-1 \cdot 10^{-3} < z/L < 1 \cdot 10^{-3}$; unstable: $z/L < -1 \cdot 10^{-3}$. The plot is based on observational data covering the whole field experiment (3 months), and simulation results from one representative diurnal cycle (1 day) with a geostrophic wind of 14 m/s.

results. Having the wall temperature and pressure gradient as the only model forcing, the day and night-time transitions are dictated by the surface temperature alone. Therefore the modeled wind speed will only drop after the surface temperature drops as well. Using the temperature distribution from figure 3, we do not expect the simulation to match the three days of measurements exactly. During a period of just three days the observed statistics might very well be influenced by large scale effects and advection. The influence of these effects is not included in the model, since the model forcing is determined based on local measurements at mast M0 alone.

Applying a constant geostrophic wind of course limits the comparability with the extracted dataset, as such perfect cases do not occur in reality. The magnitude and direction of the geostrophic wind will in reality never be constant in time. Numerical tests show that the choice of the geostrophic wind has a significant effect on the resulting ABL flow: figure 3 shows the simulated evolution of the velocity at 75 m at mast M0 for different geostrophic winds. However, with the focus on stability, we decided to compare the modeled and observed results for different stability classes, rather than adjusting the geostrophic wind to match the measurements. To evaluate the representation of stability effects in the model, non-dimensionalised velocity profiles for different stability classes are compared against the measurements. The Monin-Obukhov length determined in 10 m height is used to classify different stable and unstable conditions. Figure 4 shows the corresponding averaged velocity profiles for different stability classes. Despite the lack of data concerning the exact model forcing, the modeled results are in good agreement with the observations, and the modified CFD solver satisfactorily reproduces the effects of stability on the resulting velocity profiles.

In a second step, the ABL flow over the Benakanahalli hill is simulated. The precursor simulation described above provides the initial and transient boundary conditions: the wall temperature, the initial flow field and the lateral boundary conditions are all set according to the results obtained from the precursor simulation. The model set-up is the same as above except for the following differences: the computational domain is 5 km high using a grid of 96 vertically stretched cells (0.06 m cell height at wall; 270 m cell height at top boundary). In horizontal direction the domain has a polar shape with a radius of about 14 km and the lateral walls have inlet/outlet boundary conditions. A transient simulation is run to model one day (24 hours) over the Benakanahalli hill starting at midnight and using a 10 s numerical timestep. The lateral boundary conditions as well as the wall temperature are now updated at every timestep using the results from the precursor simulation.

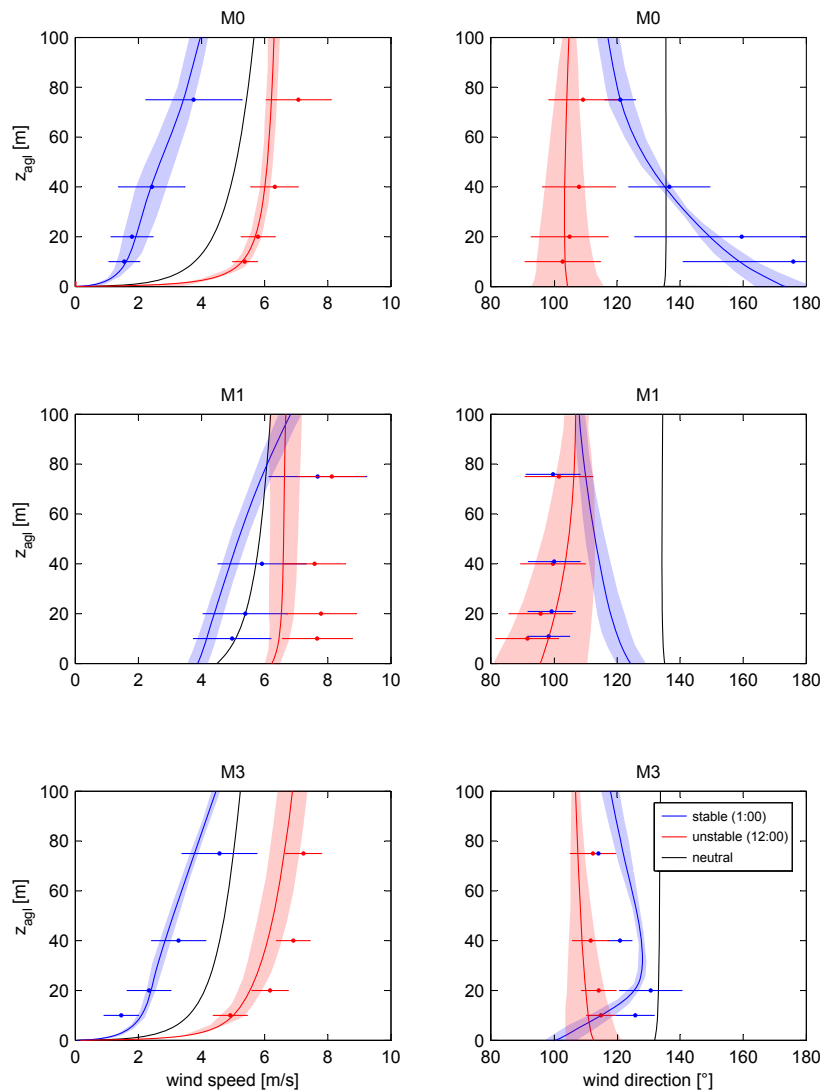


Figure 5. Velocity profiles (left) and wind directions (right) for masts M0, M1 and M3. Results from the neutral base solver (black) and the non-neutral solver compared against measurements (blue: stable conditions at 1:00; red: unstable conditions at 12:00). All data points are 40 min averages, and the error bars and shaded error regions show the corresponding standard deviation.

The idea of running a precursor simulation is to reconstruct the upstream conditions, so that the modeled flow field agrees with the observations at the upstream mast M0. However, during the observational period the upstream conditions are not ideal: for the 135° direction both the measurements and simulations at M0 indicate a significant influence of the terrain upstream (the terrain is sloping and there is a small hill and a lake located 4 km and 6 km upstream). This limits the comparability of the results as the inflow conditions at M0 are not homogeneous and it is difficult to match the modeled and observed results at the upstream mast M0.

Instead of comparing results over the whole diurnal cycle, we limit our analysis to selected cases during the day for which modeled and observed upstream conditions at M0 compare sufficiently well. Two cases are selected that show similar upstream conditions at M0 for wind speed and wind direction at 75 m and stratification at 10 m (the bulk Richardson number is used as a measure for stability): 1:00 at night, corresponding to stable conditions and 12:00 at noon, corresponding to unstable conditions (see Figure 3). Both cases are sufficiently far away from morning and evening transitions where the ABL flow is highly transient and shows large variations within a rather short time, which would further complicate the comparability of modeled and observed results.

Figure 5 illustrates the results obtained for the selected cases at the masts M0, M1 and M3.

Differences between the neutral base solver and the non-neutral solver are compared against measurements. Simulation results and measurements are available in 10 min intervals, and all data shown in figure 5 are averages over five such intervals (resulting in 40 min averages) plotted together with the corresponding standard deviations. Velocity profiles are shown on the left and the turning of the wind with height is shown on the right. The very different velocity fields during stable and unstable conditions are induced by the combined effects of stability and Coriolis force over complex terrain. These effects cause the differences between the neutral base solver and the modified non-neutral solver. This shows that the atmosphere cannot be treated as neutral and that including these effects into the CFD solver significantly improves the predicted velocity field.

5. Discussion

Comparison of simulated results against the selected observational dataset shows that the modified CFD solver performs significantly better than the neutral base solver in predicting the velocity field in non-neutral conditions. However, numerical tests show that the results are sensitive to the model forcing and the initial conditions. Adjusting the geostrophic wind to better match the measurements is certainly possible, but is not the aim of the present work. Instead, the goal is to study the combined effects of stability and Coriolis force over complex terrain during selected stable and unstable conditions, and their representation in the CFD solver. The result are qualitative comparisons of the ABL flow patterns of modeled and observed results. The available data did not allow a meaningful quantitative comparison since the wind at mast M0 is influenced by the upstream terrain, so no "undisturbed" upstream conditions are available where the airflow is in equilibrium.

Comparison against observations raises the issue of initial and boundary conditions of numerical experiments, because they are not fully determined from the available data. Perfect test cases do not occur in reality and large scale atmospheric variations influence measured statistics. Changes in magnitude and direction of the geostrophic wind e.g. influence the simulated wind field significantly. The lack of information about these parameters limits the comparability of the results.

The advantage of the chosen methodology is its general applicability as no new model coefficients are necessary. It represents a promising starting point to applying CFD solvers for wind resource assessment in non-neutral conditions.

6. Conclusions

The combined effects of atmospheric stability and Coriolis force over complex terrain are analyzed based on observations from a field experiment close to the village of Benakanahalli in India. The representation of these effects in the modified CFD solver EllipSys3D are presented and compared against measurements. Furthermore, the sensitivity of the numerical results on the forcing and the initial conditions are examined.

The developed CFD solver shows significant improvement in predicting the airflow during non-neutral conditions compared to purely neutral simulations. Both velocity profiles and the turning of the wind with height during stable and unstable conditions agree better with measurements when simulated using the non-neutral solver. The chosen methodology to implement stability and Coriolis effects into the CFD solver is a step towards simulating ABL flows over complex terrain more appropriately.

In summary our results show that the implemented modifications are applicable and significantly improve the simulated results compared to purely neutral simulations. Despite the lack of information about boundary and initial conditions and simplifications concerning the model forcing, the developed CFD solver captures effects that are missing in a purely neutral

simulation. The chosen methodology is generally applicable and no additional constants need to be specified.

Simulated results could be further improved by generating a detailed roughness map instead of using a uniform roughness. To further improve the developed CFD solver different parameterizations are possible: the k - ϵ turbulence model could be further modified [12], and [15] propose a different version of the length scale limiter. Also a variation of the Prandtl number dependant on the local Richardson number might improve the model. Furthermore, meso-scale simulations might be able to provide information on large scales and hence the necessary initial and boundary conditions for better mimicking the ABL flow around the Benanakanahalli site.

Acknowledgments

This work has been carried within the WAUDIT project (Grant no. 238576). This Initial Training Network is a Marie Curie action, funded under the Seventh Framework Program (FP7) of the European Commission. Computations were made possible by the use of the PC-cluster Gorm provided by DCSC and the DTU central computing facility. We would also like to thank the Danish energy agency (EFP07-Metoder til kortlægning af vindforhold i komplekst terræn (ENS-33033-0062)), the Center for Computational Wind Turbine Aerodynamics and Atmospheric Turbulence (under the Danish Council for Strategic Research, Grant no. 09-067216), and Vestas Technology R&D for financial support.

References

- [1] Michelsen J A 1992 Basis3d-a platform for development of multiblock pde solvers Technical report afm Technical University of Denmark
- [2] Michelsen J A 1994 Block structured multigrid solution of 2d and 3d elliptic pde solvers Technical report afm Technical University of Denmark
- [3] Sørensen N N 1995 General purpose flow solver applied to flow over hills Technical report ris-r-827(en) Risø National Lab., Roskilde, Denmark
- [4] Taylor P A and Teunissen H 1987 *Boundary-Layer Meteorol.* **39** 15–39
- [5] Berg J, Mann J, Bechmann A and Courtney M S 2010 *Boundary-Layer Meteorol.* **141** 219–243
- [6] Bechmann A, Sørensen N N, Berg J, Mann J and Réthoré P E 2011 *Boundary-Layer Meteorol.* **141** 245–271
- [7] Sørensen N N, Bechmann A, Johansson J, Myllerup L, Botha P, Vinther S and Nielsen B S 2007 Identification of severe wind conditions using a reynolds-averaged navier-stokes solver (Proceedings: The Science of Making Torque from Wind)
- [8] Koblitz T W, Bechmann A, Sogachev A and Sørensen N N 2012 Modification of cfd code to model the atmospheric boundary layer (Proceedings: 13th International Conference on Wind Engineering)
- [9] Sogachev A, Menyulin G V, Heimann M and Lloyd J 2002 *Tellus B* **54** 784819
- [10] Sogachev A and Panferov O 2006 *Boundary-Layer Meteorol.* **121** 229266
- [11] Sogachev A 2009 *Boundary-Layer Meteorol.* **130** 423–435
- [12] Sogachev A, Kelly M and Leclerc M 2012 *Boundary-Layer Meteorol.* 1–21
- [13] Launder B E and Spalding D B 1974 *Comp. Meth. Appl. Mech. Engineer.* **3** 269–289
- [14] Castro D D and Castro I P 1997 *Boundary-Layer Meteorol.* **83** 75–98
- [15] Mellor G L and Yamada T 1974 *J. Atmos. Sci.* **31** 1791–1806
- [16] Detering H W and Etling D 1985 *Boundary-Layer Meteorol.* **33** 113–133
- [17] Ulden A P V and Holtslag A A M 1980 The wind at heights between 10m and 200m in comparison with the geostrophic wind vol 1 ed E C commission L (Proceedings: Seminar on Radioactive Releases) pp 83–92
- [18] Réthoré P E and Sørensen N N 2011 *Wind Energy*
- [19] Pope S B 2000 *Turbulent flows* 1st ed (UK: Cambridge University Press)
- [20] Spalart P R and Rumsey C L 2007 *AIAA Journal* **45** 2544–2553
- [21] Blackadar A K 1962 *J. Geophysical Research* **67** 3095–3102